JOURNAL OF GEOPHYSICAL RESEARCH, VOL. 104, NO. B12, PAGES 29,113–29,131, DECEMBER 10, 1999

Volume strain within The Geysers geothermal field

Antony Mossop[1] and Paul Segall

Department of Geophysics, Stanford University, Stanford, California

Abstract. During the 1970s and 1980s, The Geysers geothermal region was rapidly developed as a site of geothermal power production. The likelihood that this could cause significant strain within the reservoir, with corresponding surface displacements, led to a series of deformation monitoring surveys. In 1973, 1975, 1977, and 1980, The Geysers region was surveyed using first-order, class I, spirit leveling. In 1994, 1995, and 1996, many of the leveling control monuments were resurveyed using high-precision Global Positioning System receivers. The two survey methods are reconciled using the GEOID96 geoid model. The displacements are inverted to determine volume strain within the reservoir. For the period 1980–1994, peak volume strains in excess of 5×10^{-4} are imaged. There is an excellent correlation between the observed changes in reservoir steam pressures and the imaged volume strain. If reservoir pressure changes are inducing volume strain, then the reservoir quasi–static bulk modulus K must be $<4.6 \times 10^9$ Pa. However, seismic velocities indicate a much stiffer reservoir with $K = 3.4 \times 10^{10}$ Pa. This apparent discrepancy is shown to be consistent with predicted frequency dependence in K for fractured and water-saturated rock. Inversion of surface deformation data therefore appears to be a powerful method for imaging pressure change within the body of the reservoir. Correlation between induced seismicity at The Geysers and volume strain is observed. However, earthquake distribution does not appear to have a simple relationship with volume strain rate.

1. Introduction

The Geysers geothermal field in northern California has been the center of significant power production since 1960. The early 1970s saw a rapid growth in output with a five-fold increase of installed generating capacity from 82 MW at the beginning of 1971 to 412 MW by the end of 1973 [*Barker et al.,* 1992]. To monitor possible crustal deformation due to the increased withdrawal of geothermal fluids, a series of geodetic surveys was carried out by the U.S. Geological Survey (USGS) and the National Geodetic Survey (NGS). These began in 1972–1973 and consisted of precise vertical and horizontal control networks that were resurveyed every 2–3 years [*Lofgren,* 1981].

Between 1973 and 1977, subsidence of up to 0.192 ± 0.022 m was measured. Horizontal movements of as much as 0.095 ± 0.007 m were observed for the period 1972–1977. The displacements were generally inward, toward the heart of the steam production area. These deformations were interpreted as contraction within the geothermal reservoir, controlled by either a poroelastic or thermoelastic process [*Lofgren,* 1981; *Denlinger et al.,* 1981]. A more recent study supports a predominantly poroelastic mechanism [*Mossop and Segall,* 1997].

In 1981 the deformation monitoring project was terminated, and much of the recorded data were scattered. However, throughout the 1970s and 1980s installed generating capacity continued to increase, reaching over 2 GW by the end of 1988. During this same period it also became apparent that reservoir steam pressures were declining, falling from an initial pressure of 3.5 MPa to as low as 1.2 MPa by 1988 [*Barker et al.,* 1992]. The drop in pressure was severe enough to cause a decline in power production and stop further increases in generating capacity within the the geothermal field.

To determine how surface deformation had progressed since the last leveling, a series of surveys, using high-precision Global Positioning System (GPS) receivers, was carried out during the summers of 1994, 1995, and 1996. These measured the locations of selected, surviving, geodetic monuments within and local to The Geysers. In this paper we use the leveling and GPS data to model the volume change within the reservoir from 1975 to 1996 (sadly, we could not obtain the earlier horizontal displacement data).

[1]Now at Institut de Physique du Globe de Paris.

Paper number 1999JB900284.
0148-0227/99/1999JB900284$09.00

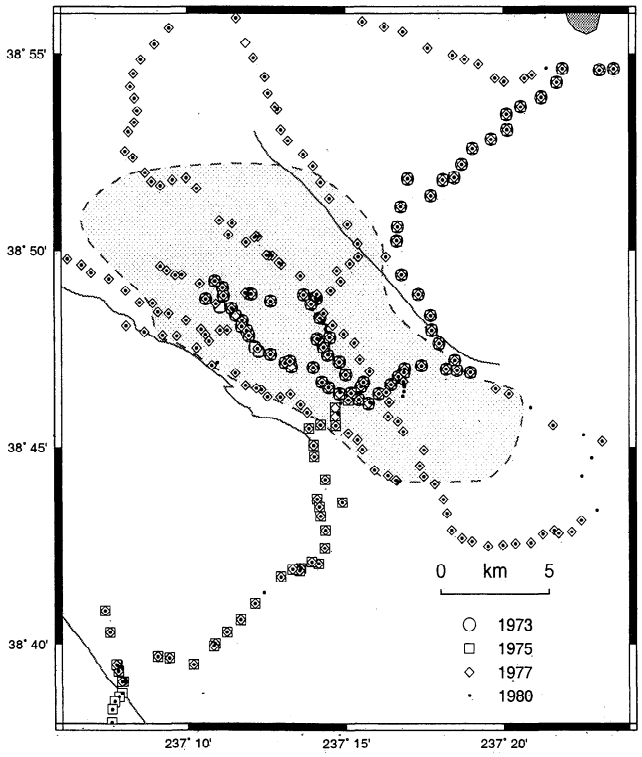

Figure 1. Location of the leveling monuments for the surveys of 1973, 1975, 1977 and 1980. The dashed line shows the California Division of Oil Gas and Geothermal Resources' (DOGGR) estimate of the reservoir boundary.

2. Leveling Surveys

The locations of the leveling survey monuments are shown in Figure 1. The initial leveling survey took place during mid-1973. It consisted of a loop following the road inside The Geysers field and a line stretching some 20 km to the northeast, terminating at the reference monument Y 626. The 1975 leveling survey measured elevations at the same survey markers (bar the inevitable few that had been destroyed) and additionally extended the line ~20 km to the southwest. The 1977 survey saw a dramatic increase in leveling coverage with the throughgoing line and inner loop surveys being augmented with several additional lines being monumented and surveyed to the north, west, and southeast. The 1980 survey, shown in Figure 1, was the largest of all, measuring elevation at all the monuments from the previous surveys (excepting losses) and extending coverage still further.

All leveling surveys were carried out to first-order, class I, specifications, with a nominal error of 4 mm per square root kilometer of level line. Open ended lines and ties were double run, while loops were single run. The fixed reference monument for each survey was Y 626. Records of the field- and temperature-corrected data survive; these were the elevations published by *Lofgren* [1981].

3. GPS Surveys

GPS satellite observables were recorded on Trimble 4000 SSE and SSI receivers using matching Trimble 4000 SSE and older SST antennae with ground planes. The antennae were mounted on brackets on wooden tripods. The mounting brackets were aligned directly over the center mark of the geodetic monuments and leveled using rotating optical plummets. The antennae were then aligned with true north and locked into place. Heights to the antennae were measured using rigid, screw-sectioned, height sticks with three measurements being made, at set up, around the edge of the antennae ground planes. Alignment and height were in this way kept to millimeter accuracy.

Data were recorded for sessions that lasted at least 6 hours and frequently 12 hours overnight. Most sites were occupied for two sessions during each survey. The sample interval was 30 s; satellites were observed for elevation angles in excess of 10°. At the end of each session the heights and alignment were remeasured and any displacement noted. Displacements were rarely in excess of 1 mm. Monuments were chosen for surveying on a combination of (i) existence (many monuments had disappeared by 1994 and two from the 1994 survey were destroyed by 1996); (ii) coverage of the region of interest and former maximum subsidence zones; (iii) unobstructed view between satellites and antenna; and (iv) accessibility. Many compromises were made and even sites among and under trees were surveyed with surprisingly good results. The majority of sites surveyed were leveling monuments.

The locations occupied in the surveys of 1994, 1995, and 1996 are shown in Figure 2. Each successive survey attempted to improve coverage over the geothermal reservoir within the limits of time, manpower, and budget. Unfortunately the reference marker Y 626 could not be surveyed because it was directly under a low tree branch.

Data analysis of the recorded satellite observables first required the correction of cycle slips and the removal of outliers in the carrier phase obervables [*Hofmann-Wellenhof et al.,* 1994; *Leick,* 1990], this was achieved using the PhasEdit carrier phase editing algorithm (J. Freymueller, personal communication, 1996). To solve for the optimum location of each antenna, GIPSY/OASIS II release 4 software [*Webb and Zumberge*, 1995] was used (hereinafter referred to as GIPSY). To automate the tedious and repetitive tasks of filtering, analyzing and re-editing involved in the processing of survey campaign data, a set of scripts were developed. The GIPSY-determined locations were estimated using (i) fixed satellite orbits, measured by the Jet Propulsion Laboratory; (ii) loosely constrained fiducial stations, ±1 km, to reduce possible translations and rotations of the surveyed network; and (iii) a high-precision, hydrogen maser, reference clock at one of the fiducial stations (Goldstone). The fiducial stations are given in Table 1;

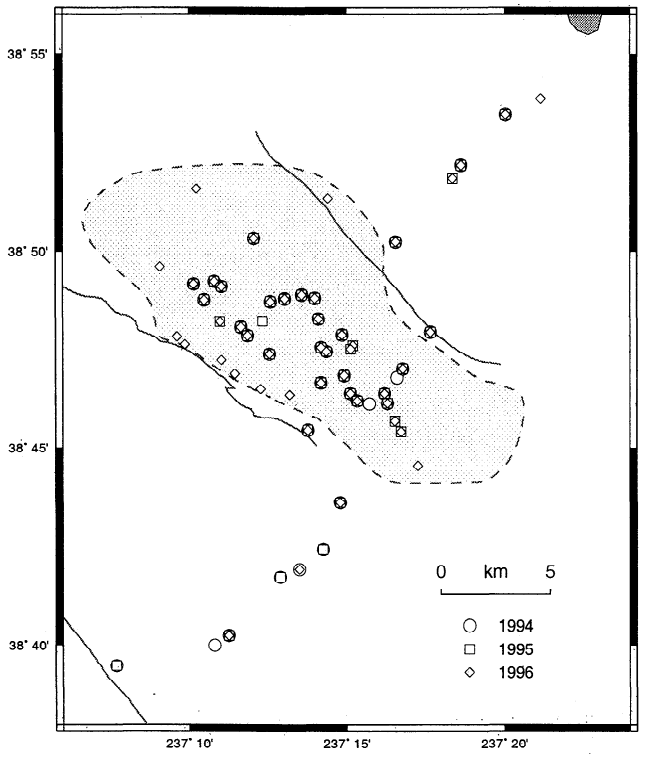

Figure 2. Monuments occupied during the GPS survey campaigns of 1994, 1995 and 1996.

they were chosen to provide a surrounding constraint about The Geysers. However, the reference frame is determined from the fixed orbits and reference clock, not from the known locations of these fiducial stations.

Comparing displacements between the 1994 and 1996 surveys holding the Briones fiducial station constant (the closest fiducial station to The Geysers, at a distance of ~100 km), apparent displacements of the order of 1–2 cm were seen in the network of fiducial stations on the North American mainland. The Hawaiian station KOKR displaced about 10 ± 4 cm. Displacements of a High Precision Geodetic Network monument some 15 km from The Geysers (HPGN 0414) for which we would expect little movement between 1994–1996 were less than a centimeter, indicating that network distortions were of long wavelength and therefore small over the short baselines, of order 10 km, considered here.

Formal data covariance matrices are calculated by the GIPSY software, and these were then scaled to match the repeatability of the station positions within the same campaign. For the 1994 campaign, covariance scaling was 3 and for 1996 it was 2. Repeatability of monument locations within each camapign was typically <1 cm for horizontal components and ~1.5 cm for the vertical.

4. Inversion Method

We assume that the surface displacements are caused by volume strain within the geothermal reservoir. To model this, we consider surface deformation of a half-space due to internal volume strain. The displacement at any surface point $\mathbf{x}$ is written as $\mathbf{u}(\mathbf{x})$ and is given by [*Okada*, 1992]

$$u_i(\mathbf{x}) = \frac{1-\nu}{\pi} \int_V \Delta\theta(\mathbf{a}) \frac{x_i - a_i}{||\mathbf{x}-\mathbf{a}||^3} d\mathbf{a}. \qquad (1)$$

Here i denotes the ith Cartesian Component; ν is Poisson's ratio; $\Delta\theta(\mathbf{a})$ is the volume strain at point $\mathbf{a}$ within the model volume V; and $||\mathbf{x}-\mathbf{a}||$ is the Euclidean length between $\mathbf{x}$ and $\mathbf{a}$.

The deforming volume can be discretized into a set of M cuboid volume elements. Within each volume element V_m, the volume strain is held constant, $\Delta\theta_m$. By making the elements small compared to the wavelength of the strain variations we can approximate the continuous strain distribution. Similarly, the displacement is sampled at a discrete set of N locations. The discretized version of (1) is written as

$$u_{ni} = \frac{1-\nu}{\pi} \sum_{m=1}^{M} \Delta\theta_m \int_{V_m} \frac{x_{ni} - a_i}{||\mathbf{x}_n - \mathbf{a}||^3} d\mathbf{a} \qquad (2)$$

where x_{ni} and u_{ni} are the ith Cartesian component of the coordinates, and the displacement, for the nth sample location.

A map view of the model grid used, in comparison to the reservoir boundary, is shown in Figure 3. The geothermal reservoir is simply a volume of hot fractured rock; it extends through a layer of Franciscan graywacke into an underlying silicic intrusive known as the felsite

Table 1. *Fiducial Stations and Their Coordinates in the WGS 84 Geodetic Datum*

Name	X (m)	Y (m)	Z (m)
Goldstone	-2353614.2928	-4641385.5143	3676976.6798
Kokee	-5543838.2274	-2054587.3602	2387809.8913
Penticton	-2059164.7790	-3621108.4749	4814432.5839
Quincy	-2517231.0979	-4198595.2531	4076531.4536
Briones	-2681173.2151	-4265460.6225	3898552.1053
Hopland	-2708981.8465	-4159579.6002	3992123.9499

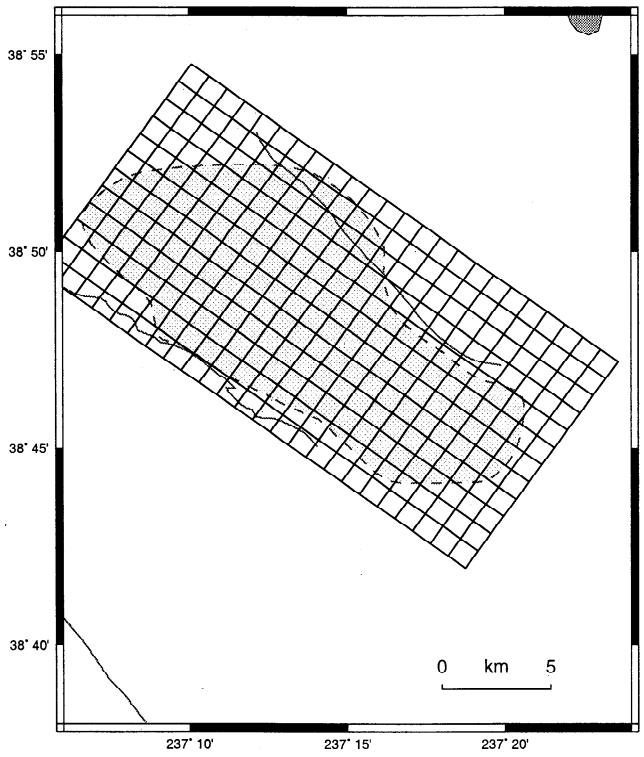

Figure 3. Map showing the top surface of the model parameterization grid. There are four layers of 1 km thickness from 0 km to 4 km below sea level (bsl).

and is capped by layers of Franciscan melange. The top of the reservoir lies on average 1 km or so below sea level but ranges from 0.3 km above sea level in the central southeast of The Geysers field to 2 km below sea level (bsl) at the edges. The bottom of the reservoir is poorly constrained but is estimated to be typically 2–3 km bsl and as much as 4 km bsl in the central northwest part of the reservoir [*Williamson*, 1992]. The model grid has four layers of 1 km thickness ranging from 0 to 4 km bsl. Each layer has 288 cubes of 1 km^3 making a total of 1152 model elements.

For each model parameter and each component of displacement at every location the integral in (2) is solved. This allows equation (2) to be written in the form

$$\mathbf{d} = \mathbf{G}\mathbf{m}, \tag{3}$$

where $\mathbf{d}$ is a vector of all the displacement components at each location; $\mathbf{G}$ is a matrix that relates each element of $\mathbf{d}$ with the vector of model parameters, $\mathbf{m}$; and each model parameter is the volume strain in its associated model volume.

To solve for the model strain, given a set of measured displacements, requires the inversion of (3). The $\mathbf{G}$ matrix and data vector $\mathbf{d}$ are first scaled by a weighting matrix $\mathbf{T}$, where $(\mathbf{T}^T\mathbf{T})^{-1}$ is the data covariance $\mathbf{\Sigma}_d$.

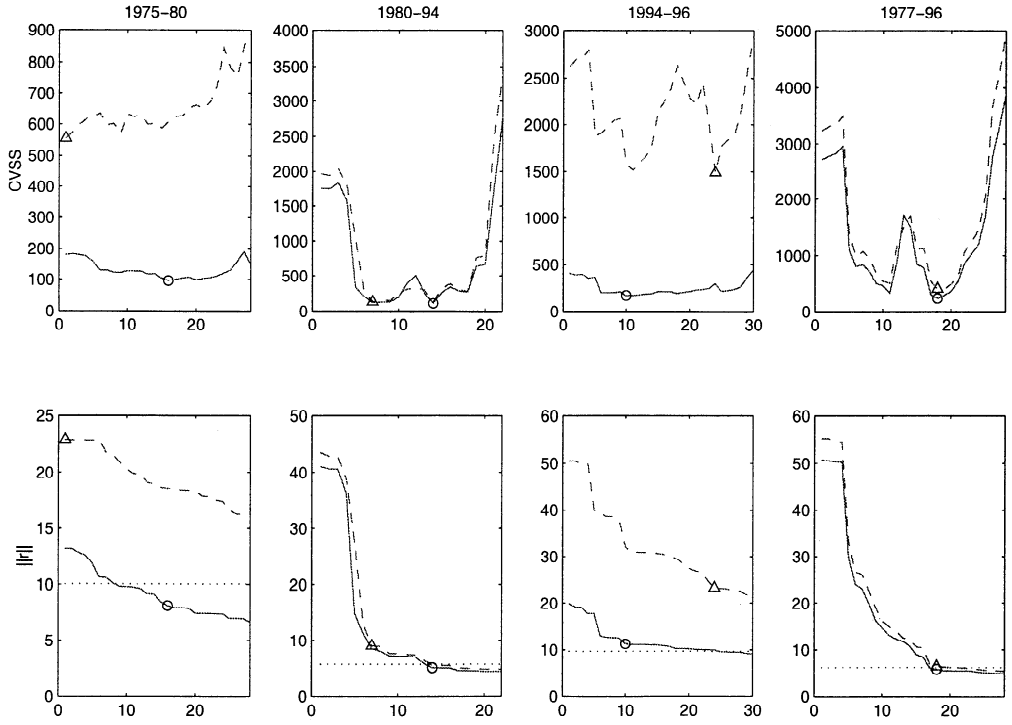

Figure 4. (top) Cross-validation sum of squares (CVSS) as a function of the number of singular values used in each of the volume strain inversions. The dashed lines correspond to a purely random walk monument instability error of 1.5 mm/$\sqrt{\text{yr}}$; the optimum number of singular values corresponds to the minimum in CVSS, marked with a triangle. The solid lines correspond to the case where the monument instability error includes the same random walk component and an additional stationary error of 10 mm; here the minimum in CVSS is marked with a circle. (bottom) Variation in the residual norm ($||r||$) for the same cases. The dotted line indicates the expected value of $||r||$ for the optimum number of singular functions.

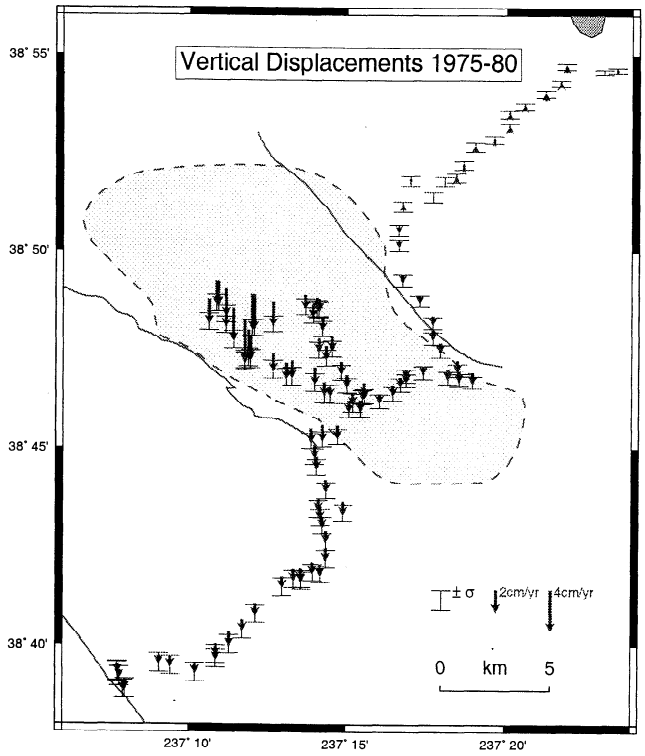

Figure 5a. a) Vertical displacement rates 1975–1980.

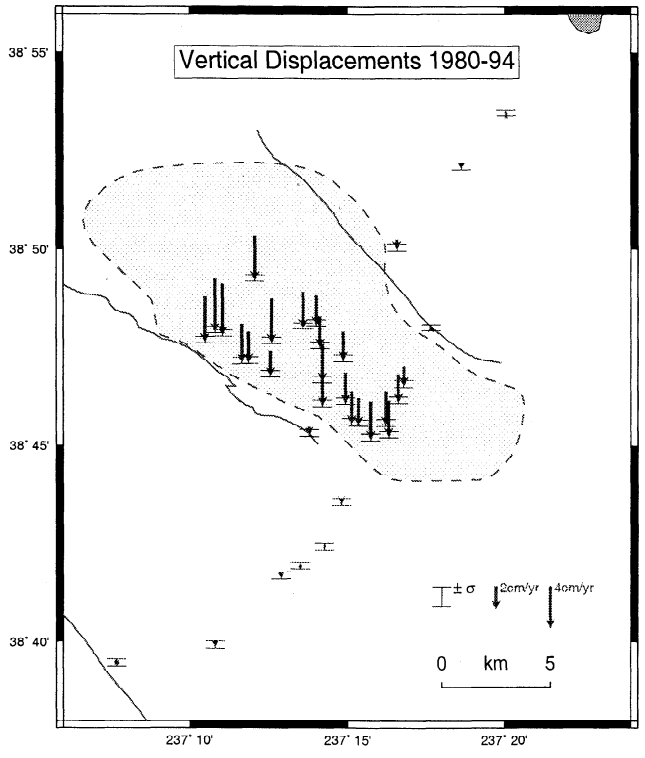

Figure 5b. b) Vertical displacement rates 1980–1994.

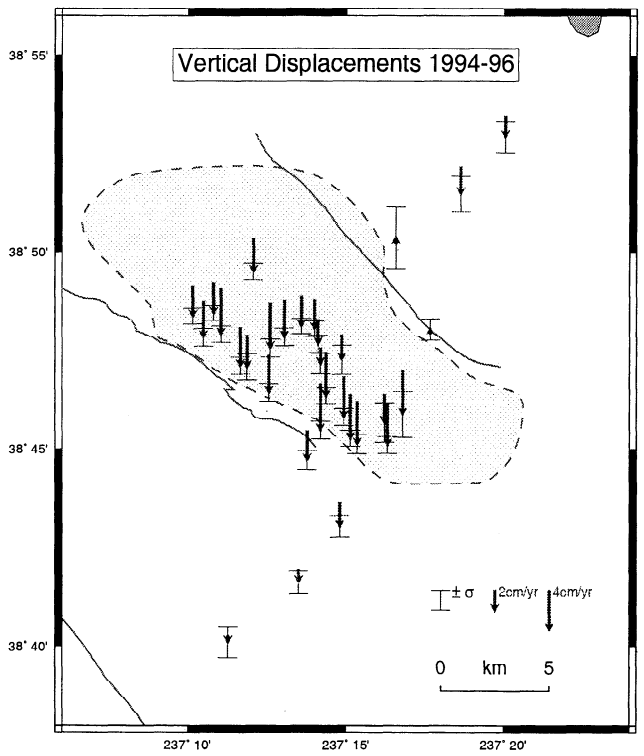

Figure 5c. c) Vertical displacement rates 1994–1996.

The inversion of the product **TG** is then achieved by using straightforward singular value decomposition (svd).

To avoid overfitting the displacement data and the errors it contains, we ignored small singular values and their associated singular vectors. The cutoff point for the singular values was determined by applying "leave one out cross validation" [*Wahba*, 1990]. This technique measures the ability of an inverse of a given complexity (where, in this case, complexity is controlled by the number of singular values and associated singular vectors retained in the solution) to predict an omitted observation given an estimate based on the $N-1$ remaining measurements. The optimal inverse is the one giving the lowest sum of squared residuals between the predicted and the omitted data values. Rather than generating N models for each truncated inverse the cross validation sum of squared residuals (CVSS), can be more easily calculated from [*Wahba*, 1990; *Matthews and Segall*, 1993]

$$\mathrm{CVSS}(\tau) = \sum_{j=1}^{N} \left[\frac{r_j(\tau)}{1 - \mathrm{diag}(\mathbf{H}(\tau))_j} \right]^2 . \qquad (4)$$

Here $\mathbf{H}(\tau)$ is the data resolution or "hat" matrix for an svd inversion truncated at τ, *i.e.*, $\mathbf{H}(\tau) = \mathbf{TG}(\mathbf{TG})^{\dagger\tau}$, where $\dagger\tau$ indicates svd inversion truncated at τ. The weighted normalized residual vector $\mathbf{r}(\tau)$ is given by $\mathbf{r}(\tau) = [\mathbf{I} - \mathbf{H}(\tau)]\mathbf{Td}$. The optimal value of τ, τ_{opt}, is simply the one that minimizes the CVSS(τ).

The singular value cutoff is then checked using the L_2 norm of the weighted normalized residual, $r_j(\tau)$. This relies on the prediction that $||r_j(\tau)||_2 > \sqrt{N} > ||r_j(\tau+1)||_2$ and is refered to as "fitting to tolerance" [*Parker*, 1994]. Both cross-validation and tolerance methods rely on the weighting matrix $\mathbf{T}$ and hence require knowledge of the data covariance $\mathbf{\Sigma}_d$.

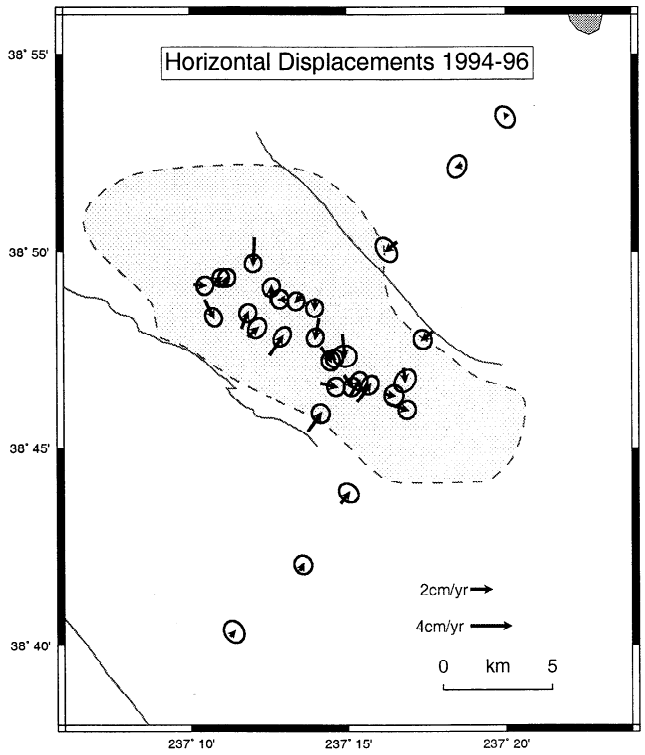

Figure 5d. d) Horizontal displacement rates 1994–1990.

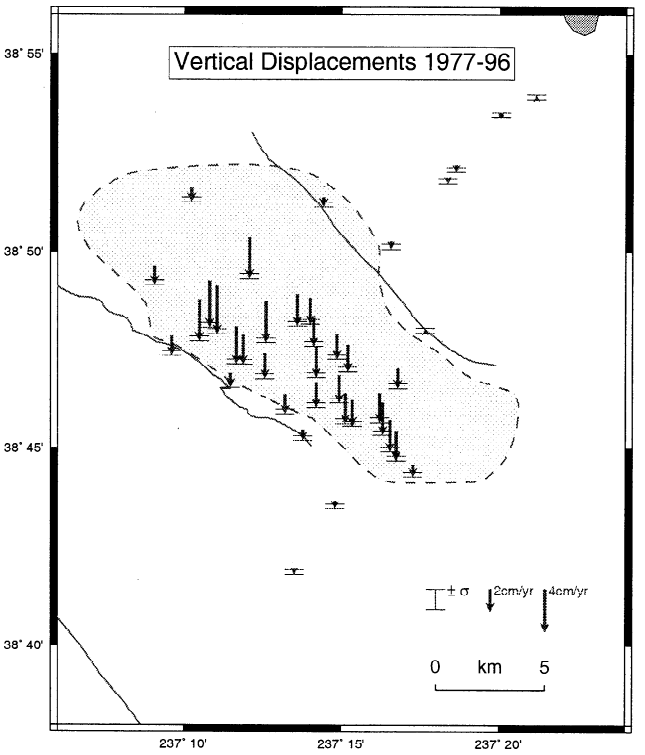

Figure 5e. e) Vertical displacement rates 1977–1996. Error bars and ellipses indicate ± 1 standard deviation.

5. Data Covariance

We examined the displacements across four epochs, 1975–1980, 1980–1994, 1994–1996, and 1977–1996. The 1973 data were poorly constrained due to the single leveling line connecting the subsiding heart of The Geysers with the exterior; hence we started with the 1975 survey (see Figure 1).

The 1975–1980 displacements simply compare leveling with leveling. Leveling elevations are calculated by summing the height differences between monuments and adding this to the known reference monument elevation. The error at any monument therefore depends on the measurement error for the preceding monuments in the survey; hence the data covariance matrix for leveling measurements, $\mathbf{\Sigma}_{dL}$, has off-diagonal terms. The weighting matrix due to leveling error in a survey, $\mathbf{T}_L$, is given by [*Arnadottir et al.*, 1992]

$$T_{L\,ij} = \frac{1}{\sigma}\left(\delta_{ij}\sqrt{\frac{1}{l_i}} - \delta_{i(j+1)}\sqrt{\frac{1}{l_i}}\right), \qquad (5)$$

where δ is Kronecker's delta function; l_i is the distance between the $i-1$th and ith monument in kilometers. The reference monument is the 0th; and σ is the error per square root kilometer of level line, nominally 4 mm for the level surveys considered here. In fact, when the loop misclosures and double run discrepancies are investigated the errors are <4 mm per square root kilometer and are closer to 2.5 mm per square root kilometer. For the weight matrix for the 1975–1980 displacements, which are calculated between two leveling surveys of equal accuracy, we multiply σ by $\sqrt{2}$.

The 1980–1994 subsidence requires the comparison of leveling and GPS survey heights. However, these cannot be directly differenced. Leveling measures elevation with respect to a geoid-based, orthometric datum, whereas GPS elevation is with respect to an idealized ellipsoidal reference frame. In this instance, the leveling surveys were with respect to the NGVD 29 datum and the GPS heights were determined relative to the WGS 84 reference ellipsoid. For comparison to be made between the leveling and GPS results they first have to be transformed into the same coordinate system.

The problem of converting geodetic reference frames is the subject of ongoing research at the National Geodetic Survey (NGS). The present state of the art geoid model is GEOID96 [*Milbert and Smith*, 1996]. GEOID-96 gives the height of the NAVD 88 geoid with respect to the NAD 83 ellipsoid and so allows conversion between these two reference frames. An additional transformation from NGVD 29 to NAVD 88 coordinates is required for The Geysers leveling data and is achieved by applying NGS's VERTCON model. The difference between the NAD 83 and WGS 84 ellipsoids is insignificant ($<10^{-6}$m for this study) compared to the errors in the GPS data, and so no further transformation is necessary. It should be noted that the GEOID96 and VERTCON models are themselves inexact and so increase the uncertainties in the computed displacements. GEOID96 has a stated error of 25 mm for baselines in

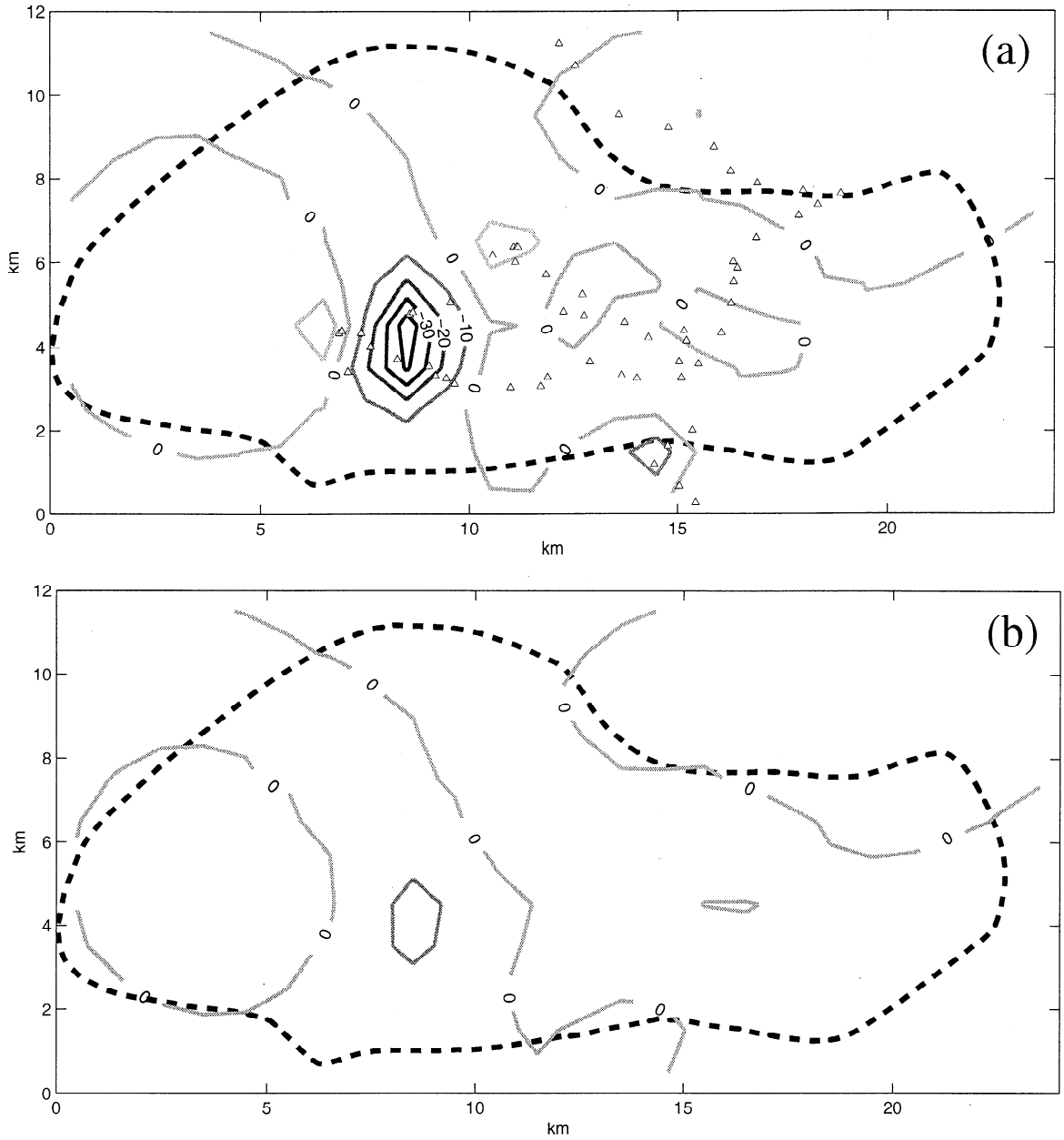

Figure 6. Modeled volume strain rate for the period 1975–1980. Strain contours are in units of 10^{-6}/yr (i.e. total strain divided by 5). (a) Layer 0 km to 1 km bsl. Monuments shown as triangles. (b) Layer 1 km to 2 km bsl.

excess of 50 km. However, because a large component of the error is correlated and tends to have a low spatial frequency, for baselines lengths <50 km the transformation error decreases. Most of the monuments are ~20 km from the reference site for which GEOID96 empirically gives transformation errors of about ±10 mm [*Milbert and Smith*, 1996; D.G. Milbert, personal communication, 1997]. VERTCON has a stated error of "<20 mm" over the coterminus United States; for the short baselines used here the transformation error is more likely to be closer to 10 mm than 20 mm (D.G. Milbert, personal communication, 1997). Hence we estimate the combined transformation error is an uncorrelated ±0.02 m at each monument, so that the transformation covariance matrix $\mathbf{\Sigma}_{dT}$ is simply $(0.02\text{ m})^2\mathbf{I}$.

The combined measurement covariance for the 1980–1994 displacements is simply the sum of the leveling, transformation, and GPS covariances. This can then be inverted and Cholesky factorized to return the combined measurement weighting matrix.

The 1994–1996 displacements compare GPS data to GPS data; hence all three components of the displacement vector can be determined, and no reference frame transformation is required. Again the weighting matrix is derived from the measurement covariance matrix by inverting and Cholesky factorization.

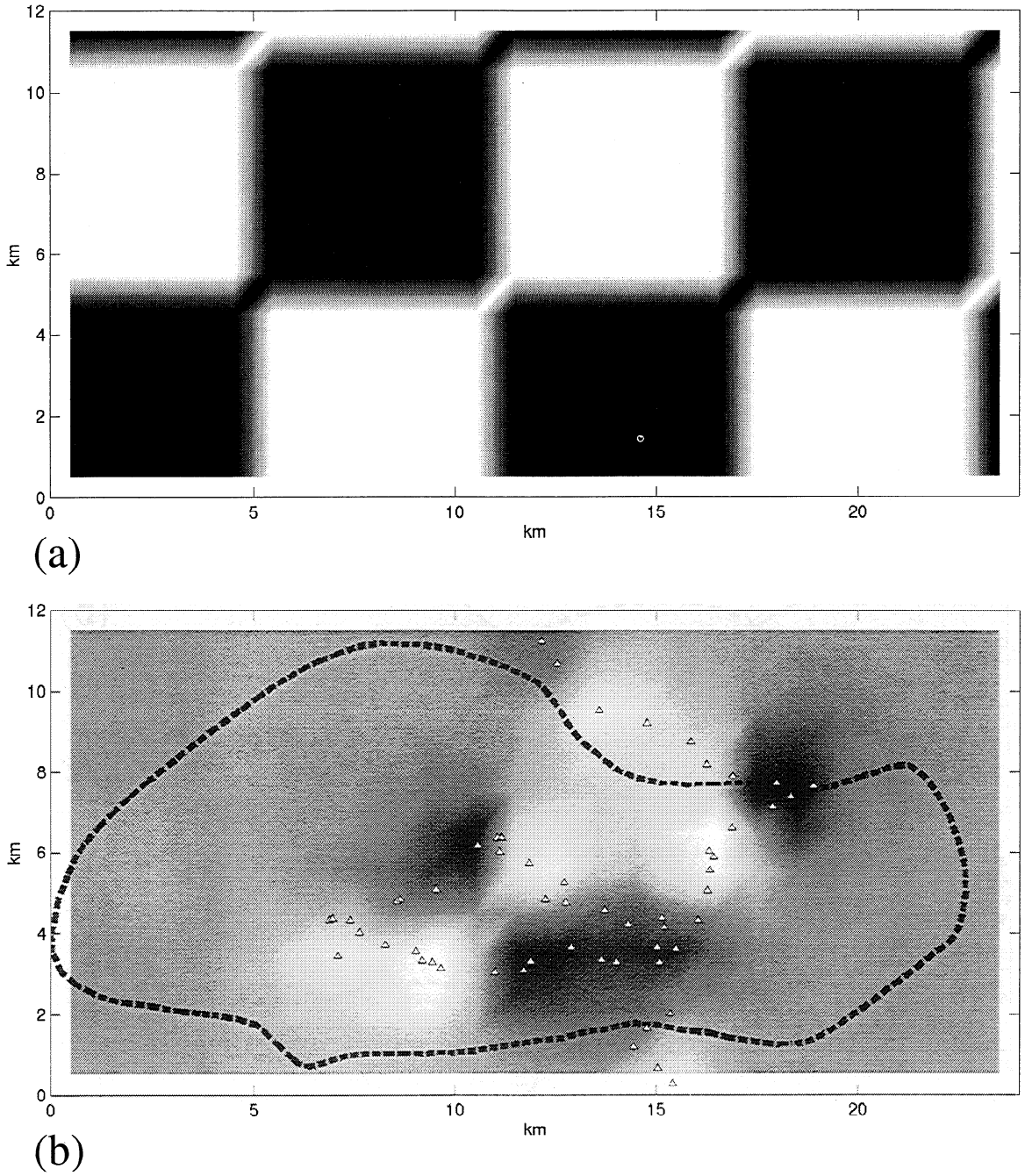

Figure 7. (a) Chequerboard pattern used for resolution test. (b) Estimated model from the chequerboard input and the svd truncation used in the 1975–1980 inversion. Note that the pattern is resolved in the center of the field where there is good monument coverage but degrades rapidly where there is little data coverage.

The 1977–1996 displacements are an attempt to look at the largest subsidence signal with the best reservoir coverage. Similar to the 1980–1994 inversion, this compared leveling and GPS measurements and so uses the same procedures described for the 1980–1994 epoch.

Monument instability also contributes to the measurement error. Many of the monuments used in this study are anchored by simple steel bar driven into the soil until refusal and are graded by the NGS as quality C, "prone to instability." *Langbein et al.* [1995] noted that monument instability for monuments of this type shows a time-correlated random walk error of $\sim$1.5 mm/$\sqrt{\text{yr}}$ as well as a variation that appeared to be controlled by seasonally occurring rainfall of as much as 10 mm.

Attempts to account for monument instability by only including the time-correlated error in this study led to large discrepancies between the cross-validation minima and the L_2 norms of the weighted normalized residuals, $||\mathbf{r}(\tau)||_2$, for the 1975–1980 and 1994–1996

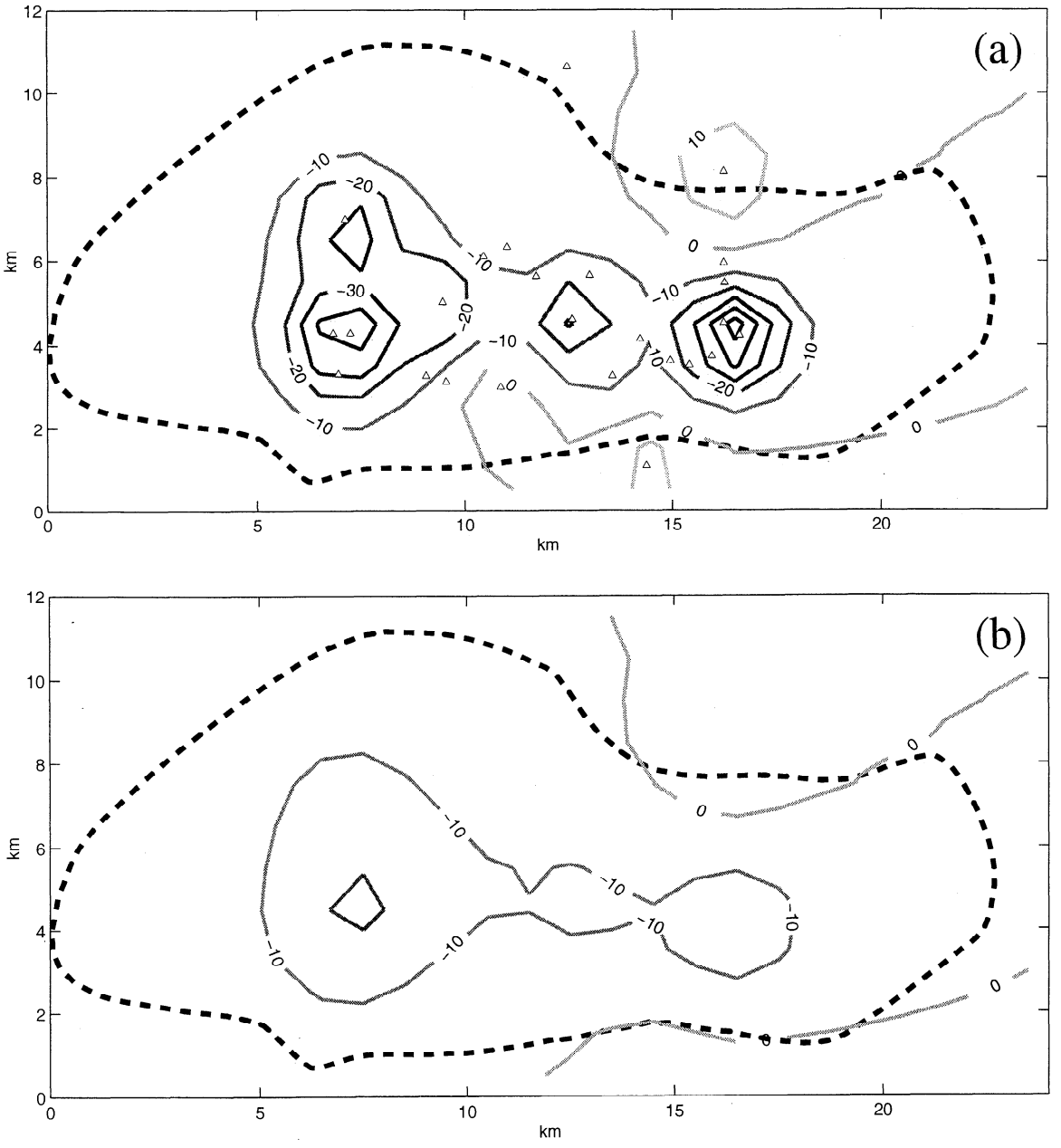

Figure 8. Modeled volume strain rate for the period 1980–1994. Strain contours are in units of 10^{-6}/yr (i.e. total strain divided by 14). (a) Layer 0 km to 1 km bsl. Monuments shown as triangles. (b) Layer 1 km to 2 km bsl.

epochs (for the 1980–1994 and 1977–1996 epochs the larger signal to noise ratios and the inclusion of estimated transformation error, ±2 cm, give better agreement). The results are shown in Figure 4 as dashed lines. Notice that for the 1975–1980 and 1994–1996 epochs, $||\mathbf{r}(\tau_{\text{opt}})||_2$, marked by a triangle, is a factor of 2 or more larger than $\sqrt{N}$, shown as the dotted line, and that for no value of τ, within the range considered, can the data be fit within tolerance. The values of $||\mathbf{r}(\tau)||_2$ for 1975–1980 disagreed with cross validation whether σ of 2.5 mm or 4 mm per square root kilometer was used.

Good agreement between cross validation and tolerance fitting methods was found by adding a time stationary error of 1 cm to all monuments to account for seasonal, setup, and other sundry errors. This is consistent with studies of monument stability by *Langbein et al.*[1995] and *Zhang et al.* [1997], although deficiencies in the model assumptions could equally explain this observation. Figure 4 shows the results of the two methods as solid lines. Here good agreement means that at least part of the range $||\mathbf{r}(\tau_{\text{opt}} - 1)||_2 \rightarrow ||\mathbf{r}(\tau_{\text{opt}})||_2$ lies within ±20% of $\sqrt{N}$ and that the interval that crosses $||\mathbf{r}||_2 = \sqrt{N}$ is only a few basis functions different from

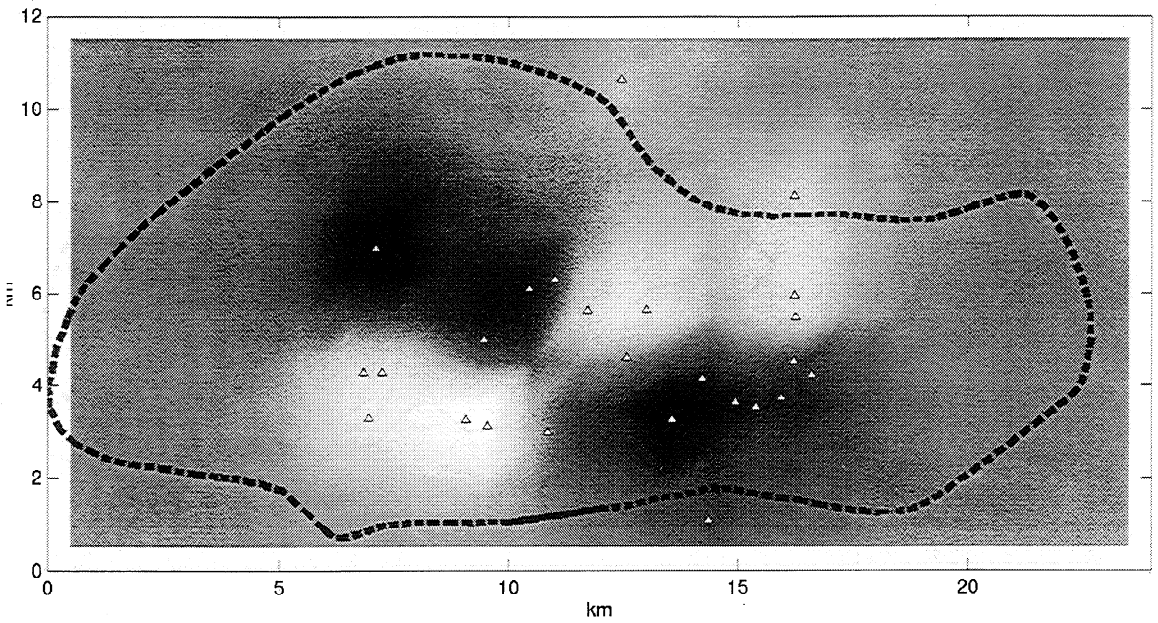

Figure 9. Similar to Figure 7b, using the same chequerboard shown in figure 7a but in this case showing the resolving power of the 1980–1994 inversion.

τ_{opt} (marked by a circle). This agreement was little affected in the 1975–1980 survey whether σ was 2.5 mm or 4 mm per square root kilometer, the former gave slightly better agreement, and as it was supported by loop misclosure and double run errors in the data, this was the value of σ chosen. The two methods now agree almost perfectly for the 1980–1994 and 1977–1996 epochs.

The tolerance matching method is much more sensitive to small changes in the data covariance than the cross-validation minima. Hence cross validation was used to determine τ_{opt} once reasonable agreement had been found. The inverted volume strain functions given below are themselves fairly robust to changes in τ_{opt}, so finding the exact value is not crucial so long as it is approximately correct. For example, for the 1977–1996 inversion the model is indistinguishable whether 16 or 21 basis functions are chosen.

6. Displacements

Figures 5a, 5b, 5c, and 5e show subsidence for the periods 1975–1980, 1980–1994, 1994–1996 and 1977-1996, and Figure 5d shows horizontal displacements for the period 1994–1996. Vertical movement is represented by north-south aligned arrows, south pointing for subsidence and north pointing for uplift. Horizontal movement is represented by arrows pointing in the direction of motion. The magnitude of each displacement is indicated by the length of arrow, the tail of which is fixed at location of the corresponding survey monument. They have all been approximately normalized by dividing by the integer number of years between surveys to show average displacements per year. The error bars and ellipses indicate ± 1 standard deviation. They are taken from the square roots of the diagonal components of the covariance matrix and have been scaled by the same integer values as the displacements.

The plots show a consistent picture of significant displacements being restricted to within, or close to, the reservoir boundary and falling off a few kilometers from the reservoir. The vertical movement is nearly all subsidence, and the horizontal displacements show inward motion toward a number of regions within the reservoir. The deformation pattern is consistent with contraction within The Geysers reservoir. In sections 7 and 8 we invert these displacement data and discuss the imaged volume strain functions.

7. Inverting the Displacement Data to Determine Volume Strain

7.1. Volume Strain for 1975–1980

For this epoch the displacements are derived from two leveling surveys. Cross validation yields a value of $\tau_{opt} = 16$ for the 1975–1980 set of displacements. The inversion results for volume strain using 16 basis functions are represented in Figures 6a and 6b. These show the upper two layers, 0–1 and 1–2 km bsl, where the majority of modeled strain occurs. The contours are in microstrain per year where the results have again been approximately normalized by dividing by the integer number of years between surveys. This normalization protocol will be repeated for all the strain results given below. However, it should be appreciated that dividing by the integer number of years between surveys is for convenience. The surveys themselves often spanned several months and were carried out at various times of year.

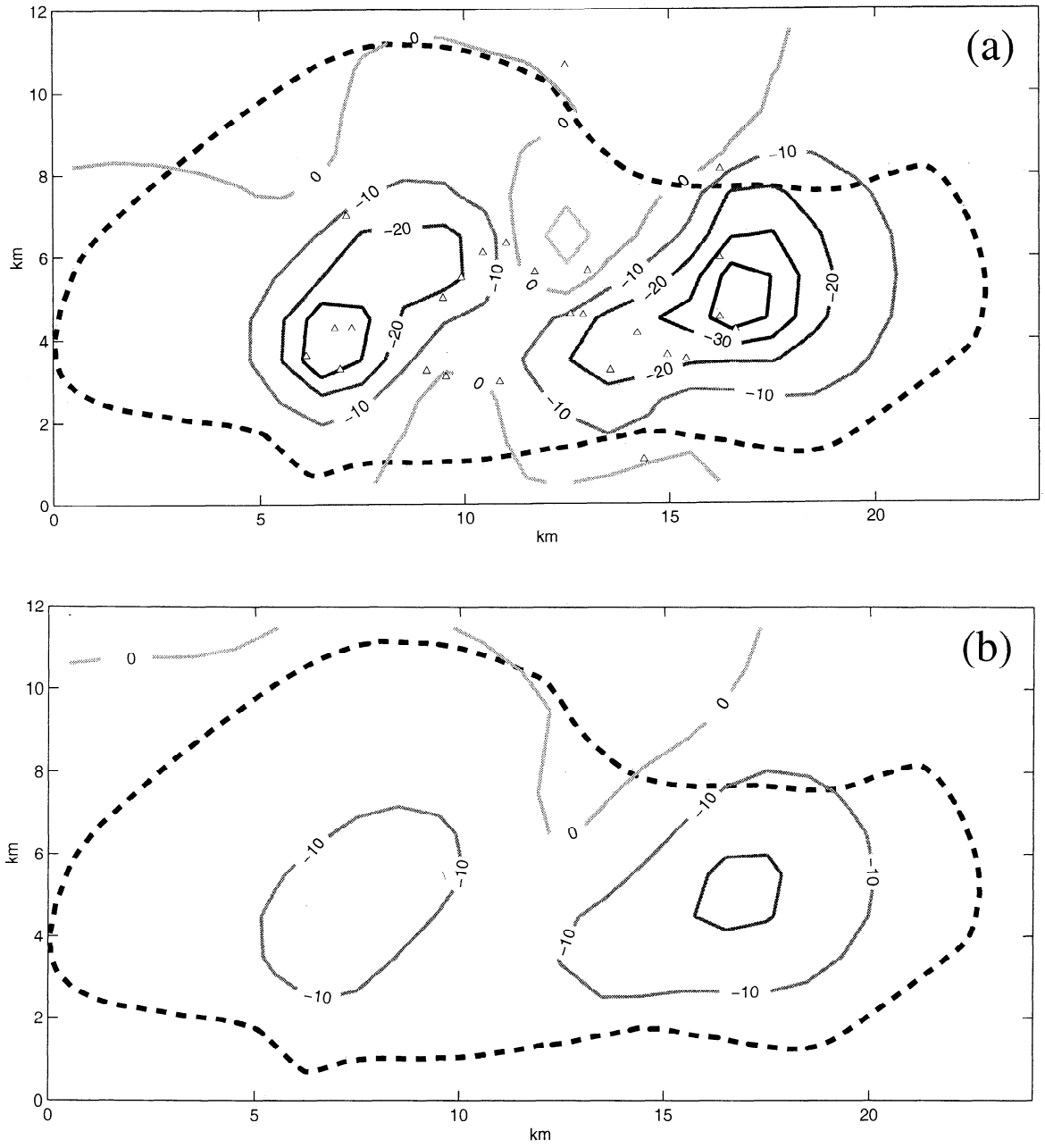

Figure 10. Modeled volume strain rate for the period 1994–1996. Strain contours are in units of 10^{-6}/yr (i.e. total strain divided by 2). (a) Layer 0 km to 1 km bsl. Monuments shown as triangles. (b) Layer 1 km to 2 km bsl.

The inversion method tends to find the minimum volume strain to explain the data; hence it is biased toward placing strain as close to the surface as possible and underestimating its magnitude. Volume strain rates of at least 40×10^{-6} yr^{-1} appear to have occurred within the reservoir in the central northwest part of The Geysers field (coordinates [9, 5]), with minor expansions to the east and north, [12, 7] and [7, 5], and a small contraction to the south, [15, 2]. If we compare monument locations with the major contraction, it can be seen that this part of the reservoir has good data coverage. The small contraction at [15, 2] is less well constrained, and its appearance at the edge of the reservoir, away from operations of that period, and its small size suggest that it is likely an artifact due to measuremnt or monument noise. Similarly, the small expansions are poorly controlled by data and are almost certainly not well resolved. To further investigate model resolution, we created a synthetic strain model of opposing maxima and minima in a chequerboard pattern shown in Figure 7a, multiplying this by the model resolution matrix, $\mathbf{R} = (\mathbf{T}^T\mathbf{G})^{\dagger_T}\mathbf{T}^T\mathbf{G}$, gives an indication of how well details are resolved by the inversion used. The results for the top layer of the model, 0–1 km bsl, are

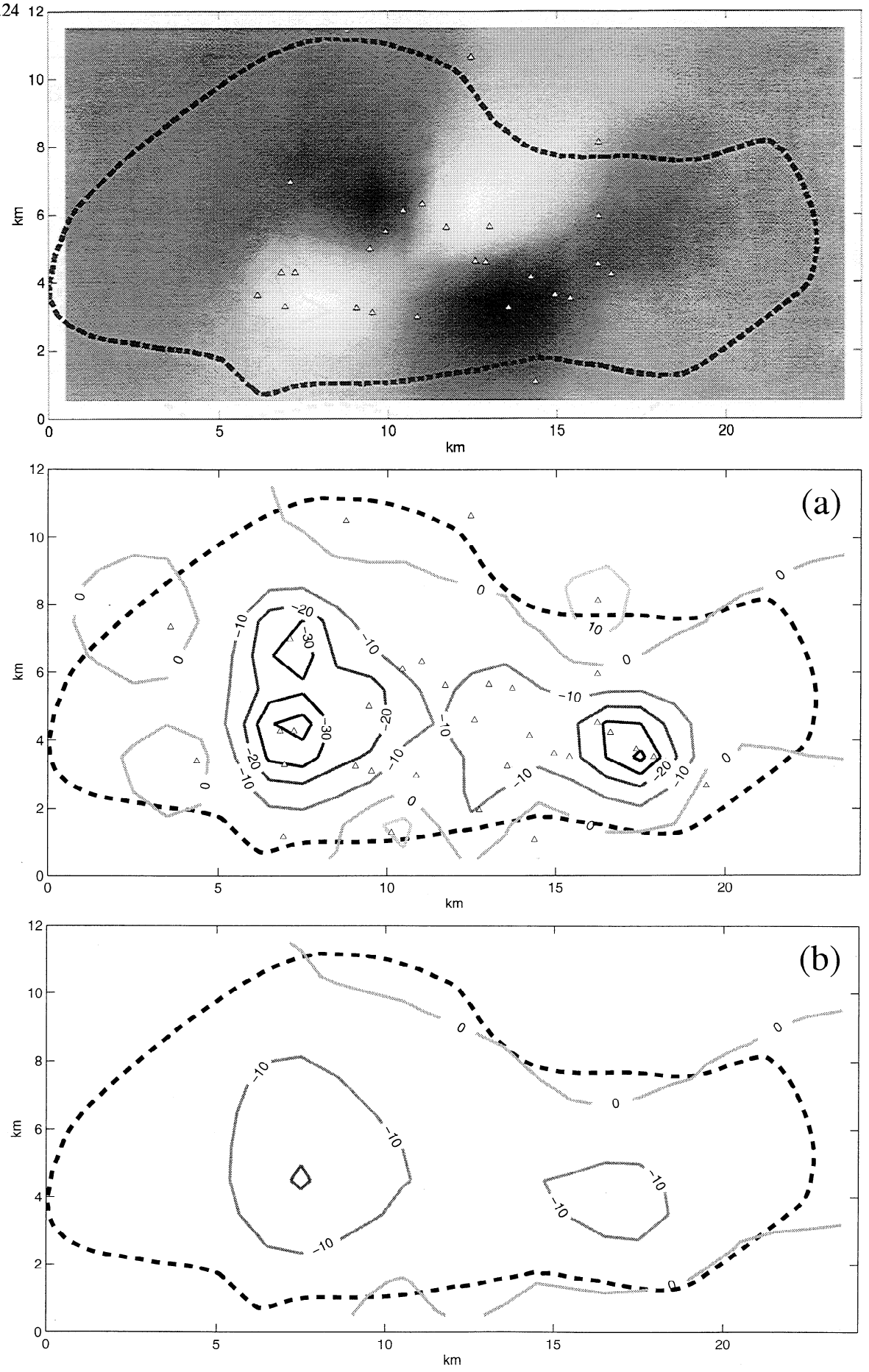

Figure 12. Modeled volume strain rate for the period 1977–1996. Strain contours are in units of 10^{-6}/yr (i.e. total strain divided by 19); (a) Layer 0 km to 1 km bsl. Monuments shown as triangles. (b) Layer 1 km to 2 km bsl.

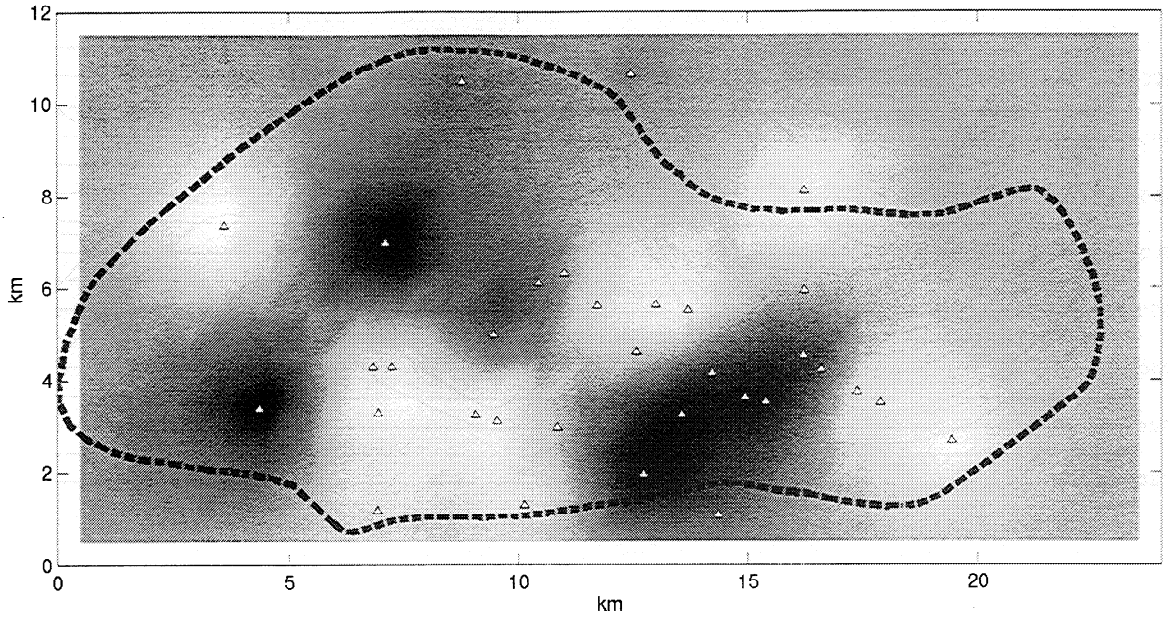

Figure 13. Chequerboard resolution for the 1977–1996 inversion.

shown in Figure 7b. While those parts of the reservoir with little monument coverage are not at all well resolved, the central part appears to have good resolution, indicating that the main volume contraction is a well-resolved feature.

The value of τ_{opt} is unchanged if we use the nominal leveling error of 4 mm per square root kilometer and the resulting volume strain model is almost indistiguishable. Even if we further neglect to include the time stationary monument error of 1 cm, we get essentially similar results, i.e., a volume contraction of $>30 \times 10^{-6}$ yr^{-1} in the northwest central Geysers (note $\tau_{opt} = 10$ for this case). The indication therefore is that the modeled volume strains are fairly robust results.

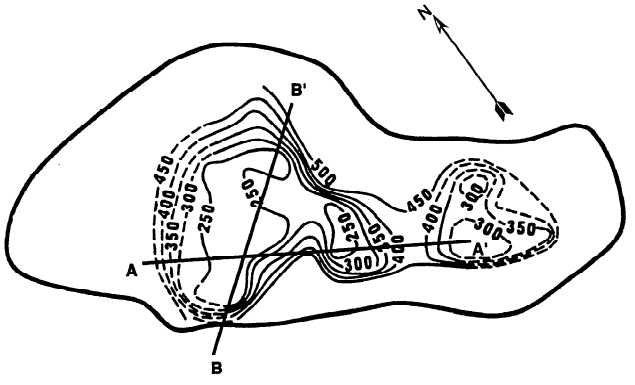

Figure 14a. Mapped pressures as of 1987 [*Williamson,* 1992] and the trace of two sections, A–A' and B–B', across this map; pressure in psia (1 psia = 6895 Pa).

7.2. Volume Strain for 1980–1994

This epoch compares the 1980 leveling and 1994 GPS observations. Cross validation indicates that 14 basis functions should be used (Figure 4). The volume strain rates shown in Figures 8a and 8b exhibit a more complex pattern. Three centers of volume contraction are imaged inside the reservoir, [8, 5], [13, 5], [17, 5], with a minor contraction at [8, 7], and a minor volume expansion to the east of the reservoir, [17, 9]. From the monument coverage it appears that the two northern volume contraction zones have reasonable coverage and that while the southern contraction source lacks constraining data on its southern side, it is controlled by several measurements to its north. The eastern maximum is seemingly only controlled by a single monument to the west of it (106 M). The model resolution is shown in Figure 9 and also suggests that while the central Geysers reservoir is quite well resolved, those areas with low monument coverage are not.

7.3. Volume Strain for 1994–1996

In this epoch the displacements are derived fully from GPS measurements. For this inversion, cross validation returns an optimum cutoff of $\tau = 10$ (Figure 4). The approximate volume strain rates for 0 1 and 1 2 km bsl are contoured in Figures 10a and 10b. These show two contraction sources, one in the central northwest, [7, 4], and one in the southern part of the field, [17, 5]. Monument coverage indicates that the southern contraction source is not as well controlled as the source to the north, but both zones have reasonable coverage. The model resolution matrix shown in Figure 11 again shows good resolution for those areas with monument cover-

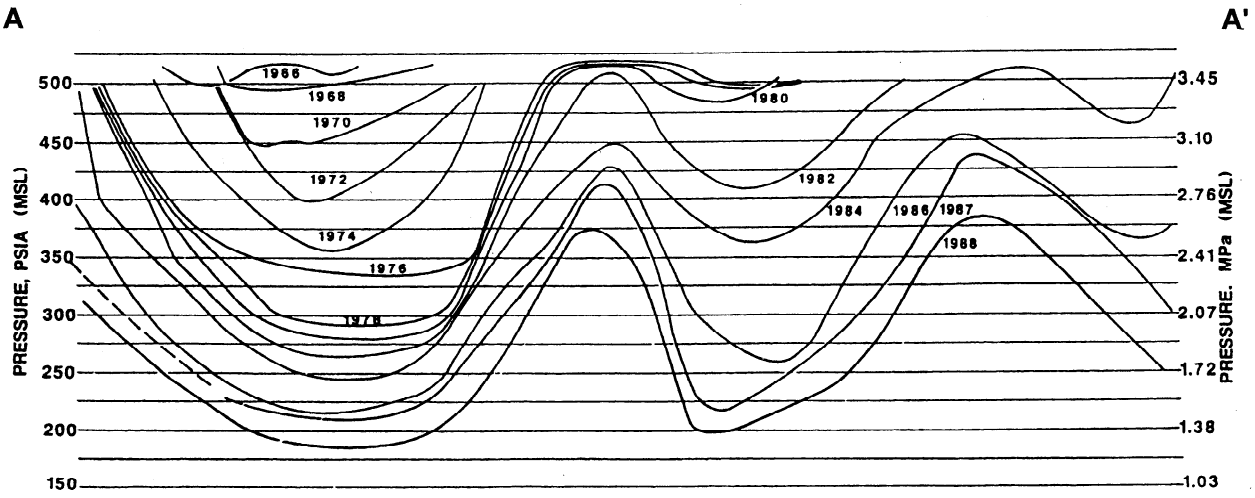

Figure 14b. Pressure evolution across the section A–A' [*Barker et al.,* 1992].

age and suggest that both the volume strain sources are well resolved.

7.4. Volume Strain for 1977–1996

This 19 year interval employs the most extensive leveling and GPS surveys. Here the best cutoff in singular values is found to be for $\tau = 18$ (Figure 4). The four volume contraction zones seen in the 1980–1994 inversion (see Figure 8a) are also clearly imaged in Figures 12a and 12b. There are also a number of maxima imaged about the margins of the reservoir. Monument distribution is also similar to the 1980–1994 epoch with somewhat better coverage at the reservoir margins. The volume contractions all have reasonable monument coverage, with the possible exception of the northeast minimum, [8, 7]. The maxima all appear to be controlled by single monuments. The resolution test plot shown in Figure 13 indicates that the central reservoir where the four minima are located is well resolved but that the maxima are in areas where the resolution is not good, with the exception of the volume increase imaged on the western edge of the reservoir.

8. Discussion

Figure 14a is a map of the reservoir steam pressure measured in The Geysers in 1987 [*Williamson,* 1992]. The measurements were taken at selected wells and correspond to the steam pressure within the highly conductive fractures that control fluid flow in the reservoir. Also shown are two pressure evolution sections across the reservoir. These sections, **A–A'** and **B–B'** (Figures 14b and 14c), show how the reservoir pressure changed from 1966 to 1989 across these lines [*Barker et al.,* 1992].

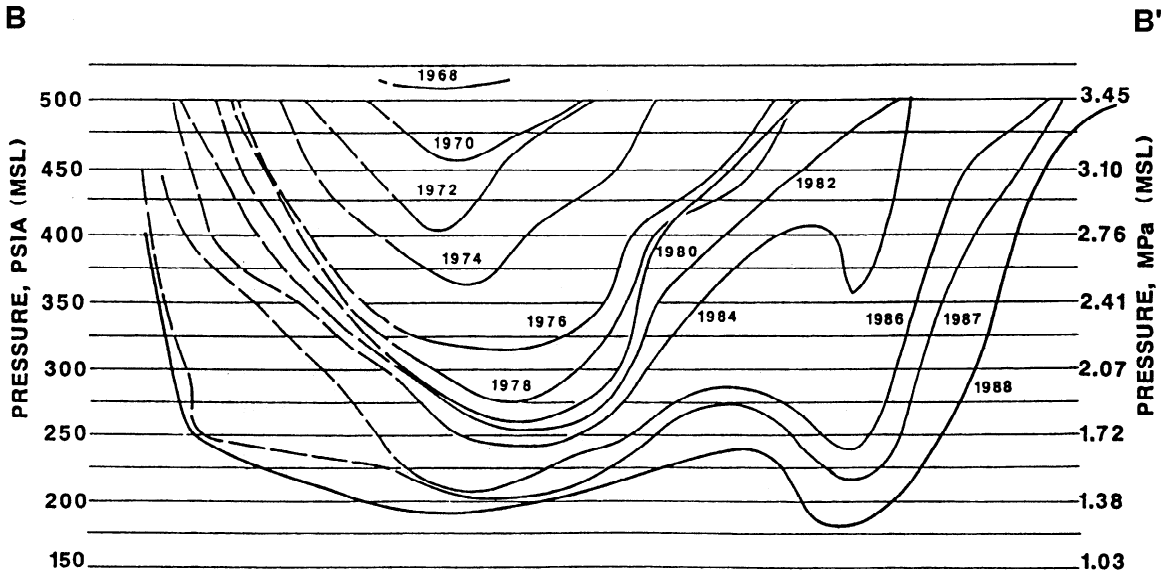

Figure 14c. Pressure evolution across the section B–B' [*Barker et al.,* 1992].

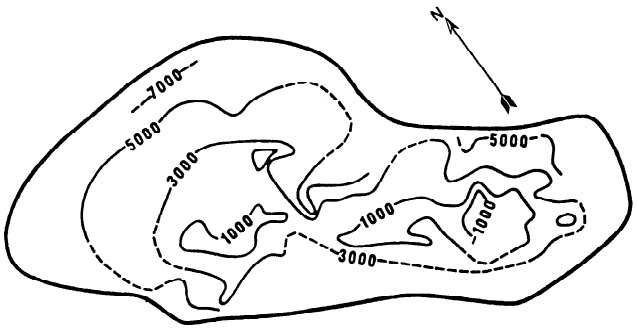

Figure 15. Map showing the estimated top of the geothermal reservoir at The Geysers field. Depth given in feet below sea level (1 foot = 0.3048 m) [*Williamson*, 1992].

There is a striking similarity between the mapped pressures (Figure 14a) and the volume strain between 0 and 1 km bsl for 1977–1996 (see Figure 12a). This suggests that there is a direct relationship between steam pressure and volume strain. Looking more closely, there is good agreement between the volume strain minimum that formed between 1975 and 1980 (Figure 6a) that lay in the northwest central Geysers, [9, 5], and the pressure low that appears to have developed in the same region over that period, (see Figures 14b and 14c). Between 1980 and 1994 the volume strain shows four minima (Figure 8a), one just to the northwest of that imaged in Figure 6a with a companion a couple of kilometers to the northeast, one in the central Geysers and one in the southeast Geysers ([8, 5]; [8, 7]; [13, 5]; [17, 5]). These again show good agreement with the locations of pressure lows shown in Figures 14a, 14b, and 14c where the pressure low of 1980 deepens and broadens to the northwest and forms a second cusp to the northeast and further pressure lows form in the central and southeast parts of the reservoir.

However, while the regions of reduced pressure and volume contraction match spatially, there appears to be a discrepancy with respect to relative magnitude. The minima in steam pressure in the northeast, central, and southeast Geysers, which formed in the period 1980–1987, are all of roughly the same intensity (Figure 14a). The pressure change between 1980 and 1987 in the northwest, however, is smaller due to the already significantly reduced pressures in that area as of 1980. In comparison, the volume strain minima show a wider range in realtive magnitude and do not seem to reflect the relative strengths predicted from pressure change. For example, the southern volume strain minima, [17, 5], for 1980–1994 is far more intense than that in the central Geysers [13, 5].

On reflection this discrepancy is not surprising, even if we discount the obvious explanation that pressure changes up to 1987 (Figure 14a) might not correspond to pressure changes up to 1994. The northeast and central pressure lows extend over smaller areas than those in the northwest and southeast. The parameterized volume strains are average values over 1 km^3 blocks within the reservoir, and model resolution appears to be over longer length scales than this. As deformation length scales approach resolution limits, inversion results tend to better constrain the volume integral of the volume strain rather than the extent or amplitude of the strain signal. Thus there can be a trade-off between amplitude and extent of the individual contraction zones. Similarly, it should be realized that the pressure measurements themselves only reflect conditions in the large

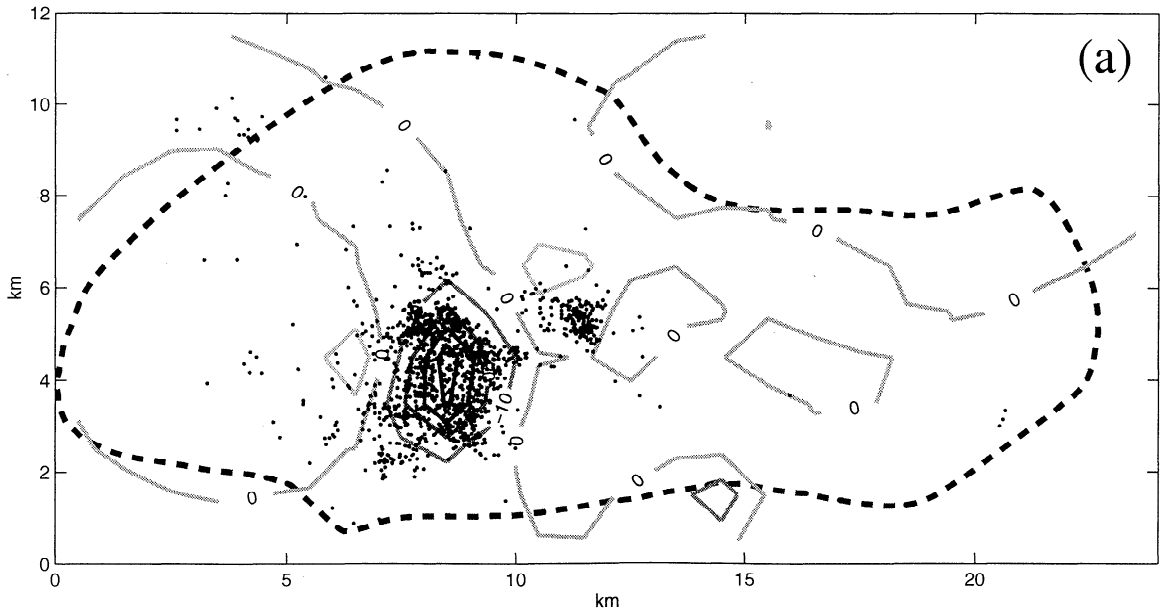

Figure 16. Plots showing earthquake activity $M_c \geq 1.4$ in relation to imaged volume strain for the periods (a) 1975–1980, (b) 1980–1994, and (c) 1994–1996.

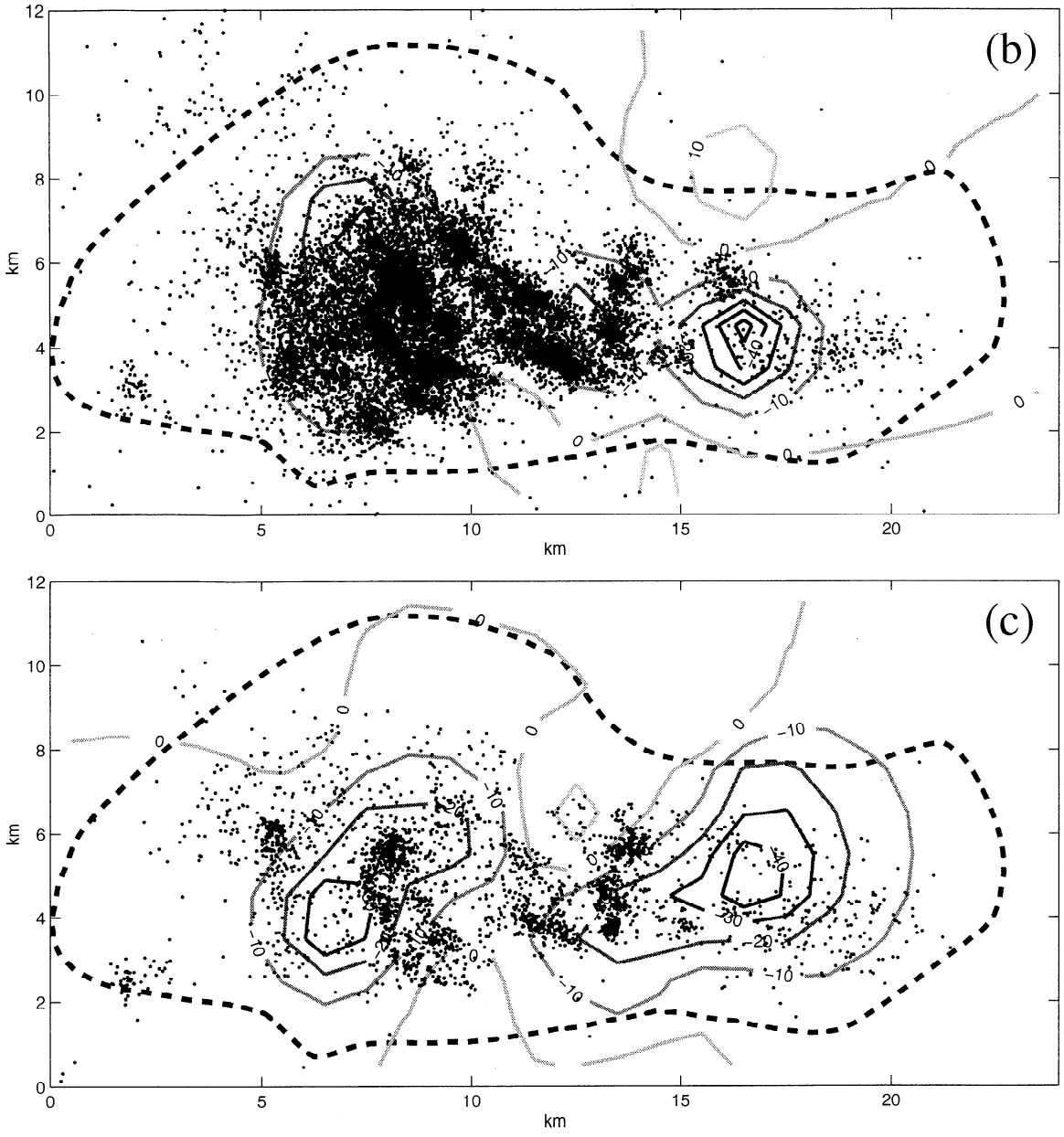

Figure 16. (continued)

conductive reservoir fractures. These large fractures control steam flow but have negligible total volume, whereas poroelastic volume strains depend on average pressures within the main body of reservoir rock.

Also, as was noted in section 7, the inversion method tends to image volume strain as close to the surface as the data and model permit, even though the actual strain may be distributed over some depth range. So areas where contraction occurs over a greater depth range will show higher apparent volume strains in the top layer of the model. The actual thickness of The Geysers reservoir is not well constrained, but evidence from microseismicity indicates that in the vicinity of the northwest pressure low the reservoir extends to as much as 4 km bsl as compared to typical depths of 2–3 km bsl [*Williamson,* 1992].

Finally, it should be noted that for each inversion we have used a half-space model with the free surface placed at the median elevation of the monuments surveyed. For 1980–1994 this was −850 m bsl (850 m above sea level), and the top of the reservoir is constrained to 0 km bsl. While the top of the reservoir is below 0 km bsl for most of The Geysers field, it does shallow to −300 m bsl in the region of the southeast pressure low (see Figure 15). The shallower the volume strain, the larger the displacements it produces (equation (1)). So constraining shallow strain to be imaged significantly deeper will cause an apparent increase in strain magnitude, as the

inversion attempts to match the surface displacements. Hence volume strain for the southeast minimum may be slightly oversestimated. Figure 15 also shows that the top of the reservoir is at shallow depth in the approximate area of the northwest pressure/strain minima. A much smaller area of shallow reservoir also occurs at the location of the northeast minima, but there is no shallowing of the reservoir associated with the central minima. This suggests the possibility that the observed relative magnitudes of the volume strain minima are in part due to variation in depth to the top of the reservoir and relief of the surface topography.

The above arguments show that it would be unrealistic to attempt to map volume strain into pressure change via a simple conversion constant throughout the reservoir. However, this does not preclude us from constraining some of the governing poroelastic parameters.

For homogeneous isotropic porous rocks (homogeneity here meaning that length scales considered are much greater than pore length scales) the quasi-static bulk modulus K is given by [*Nur and Byerlee*, 1971]

$$K = \left(\frac{\Delta\theta}{\Delta P} + \frac{1}{K_s} \right)^{-1}, \tag{6}$$

where K_s is the bulk modulus of the mineral grains that make up the rock. For The Geysers the reservoir is composed of graywacke and silicic intrusives, so we assume $K_s \approx 3.7 \times 10^{10}$ Pa, the value for quartz [*Mavko et al.*, 1996]. Arguments given above show that the volume strain is not particularly well constrained. However, for the 1980–1994 period (see Figure 8a) it is reasonable to state $\Delta\theta_{\max} > 5 \times 10^{-4}$ as a conservative lower bound, where $\Delta\theta_{\max}$ is the maximum volume strain observed. Maximum pressure changes over this period are within the bound $\Delta P < 2.6 \times 10^6$ Pa. Equation (6) returns a value of $K \leq 4.6 \times 10^9$ Pa.

This is a very low value for the bulk modulus of rock when compared to the typical values given in tables of physical constants, which are generally an order of magnitude larger. However, it should be recognized that the bulk modulus K, measured here is for low frequency, quasi-static deformations. The bulk moduli given in tables of physical constants are usually determined only for very rapid, dynamic deformation. For quasi-static strains a porous solid has an effective bulk modulus, K_{eff}, given by [*Mavko et al.*, 1996]

$$K_{\text{eff}} = \left(\frac{1}{K_s} + \frac{\phi}{K_\phi} \right)^{-1}, \tag{7}$$

where ϕ is the porosity and K_ϕ is the bulk modulus of the pore structure. The deformation is assumed to be slow enough that the pore fluid can leave the pore space, and hence there is no change in the pore pressure. This is often referred to as drained conditions and is equivalent to homogeneous pore pressure change. The Geysers has a fracture porosity of about ~1–2% [*Barker et al.*, 1992] (of this, only a small proportion is contributed by the conductive, steam-producing fractures [*Gunderson*, 1992]). Studies of natural rock fractures find $K_\phi \approx 3\sigma_n$ [*Evans et al.*, 1992]. For The Geysers reservoir it seems reasonable to estimate $\sigma_n \approx zg\rho$, where z is the depth of rock ~1 to 5 km, g is the acceleration due to gravity ~10 m s^{-2}, and ρ is the rock density ~2.7×10^3 kg m^{-3}. Hence equation (7) gives $K_{\text{eff}} \approx 3.6$–$20 \times 10^9$ Pa. The lower end of this range corresponds to deformation at the shallower reservoir depths and appears to be consistent with our subsidence derived value of K.

O'Connell and Johnson [1991] observed seismic velocities for The Geysers reservoir of $V_p \approx 4.8 \times 10^3$ m s^{-1} and $V_s \approx 2.8 \times 10^3$ m s^{-1}. These velocities correspond to a dynamic bulk modulus, $K_d = 3.4 \times 10^{10}$ Pa. The seismic propogation velocities, though, are measured for deformation frequencies in the range of 10–100 Hz, not quasi-static strains. For high-frequency deformations the elastic properties of the pore fluid become important because the fluid cannot drain from the pore space quickly enough to prevent significant changes in pore pressure occurring. Deformation frequencies for which this is the case are defined as those greater than a critical frequency f_c, which is given by [*Mavko et al.*, 1996]

$$f_c = \frac{kK_{fl}}{\eta L_c}, \tag{8}$$

where k is the permeability, ~5–100×10^{-15} m^2 for The Geysers reservoir as a whole [*Williamson*, 1992], K_{fl} is the bulk modulus of the pore fluid, η is the pore fluid viscosity, and L_c is the critical fluid diffusion length scale. At The Geysers the pore fluid in the important highly conductive fractures is steam, but these represent only a small proportion of the entire fracture porosity. Most of the fracture porosity is contained in poorly conductive fractures and microfractures where the pore fluid is water [*Gunderson*, 1992]. Therefore the appropriate value for K_{fl} is 2.5×10^9 Pa, the bulk modulus of water; η is the viscosity of water, 10^{-3} to 10^{-4} kg m^{-1} s^{-1}; and L_c is the distance water has to travel to escape to a drainage channel which is roughly the distance between steam filled fractures ~100 m. Hence seismic frequencies of 10–100 Hz $\gg f_c$, so that $K_\phi \to K_{fl}$ in (7). This then gives an estimated dynamic bulk modulus of $K_d \approx 2.9$–3.2×10^{10} Pa, in good agreement with that derived from seismic propogation velocities, (*Mossop and Segall* [1997] give an alternative explanation that relies on the smallest seismic wavelengths being smaller than L_c). Our seemingly low quasi-static bulk modulus K, therefore appears to be quite consistent with the observed seismic velocities and much larger dynamic bulk modulus K_d.

The Geysers region is also the center of a great deal of seismic activity [*Hill et al.*, 1990]. It is to be expected that fault slip in a highly fractured region would be

influenced by significant volume strains. Figures 16a, 16b, and 16c show seismicity, $M_c \geq 1.4$, for the periods 1975–1980, 1980–1994, and 1994–1996 superimposed on their respective maps of modeled volume strain between 0 and 1 km bsl. The magnitude cutoff was chosen to give complete coverage of The Geysers, i.e., all events with $M_c \geq 1.4$ that occurred in the study area are believed to have been recorded; for smaller events the spatial coverage is not complete.

There is a reasonable correlation between the volume contraction imaged for 1975–1980 and seismicity. For the period 1980–1994 there is good correlation between the volume contractions and seismicity, but there is a noticeable difference in number of earthquakes across the region. The central and northern volume contractions are associated with a large number of earthquakes. The southern contraction, while associated with a definite increase in seismicity (compare 1977-1980), does not have as many earthquakes in its vicinity. In 1994–1996 the correlation between earthquakes and volume contraction is again apparent, though somewhat weaker, with the same decrease in numbers from north to south.

Earlier studies by *Eberhardt-Philips and Oppenheimer* [1984] noted a correlation between industrial activity and earthquakes at The Geysers. Their work showed an apparent correlation between fluid withdrawal and seismicity. The close match of seismicity to volume strain would seem to confirm this finding. However, it does not identify the causitive mechanism. Further research (A. Mossop and P. Segall, manuscript in preparation, 1999), indicates that a significant proportion of the shallow seismicity is induced by the poroelastic contraction of the reservoir increasing shear stress on optimally oriented fractures in the overlying rock.

9. Conclusions

Surface deformations recorded over the period 1975–1996 at The Geysers geothermal field are consistent with volume contraction within the reservoir. The distribution of volume strain can be determined by inverting the displacement data, although the depth resolution is limited. Contraction within the reservoir appears to have followed industrial exploitation of the geothermal field, mainly occurring in the northwest in the 1970s and then spreading to the south [*Barker et al.*, 1992]. Volume strains in excess of 5×10^{-4} are imaged over the 20 years or so of this study.

There is a good spatial correlation between reduction in measured pressure and volume strain. However, unlike measured pressure, which only determines steam pressures in the conductive fracture network, volume strain is related to the pressure field throughout the reservoir volume. The conductive fracture network contains an almost negligible fraction of the reservoir pore space. Imaging the volume strain therefore gives a powerful method for determining the pore pressure change within the bulk of the reservoir.

By relating changes in measured steam pressure, which gives an upper bound on pressure changes within the bulk reservoir, to volume strain, the quasi-static bulk modulus K is estimated. A value of $K \leq 2.4 \times 10^9$ Pa is found. This apparent compliance is consistent with the physical properties of the reservoir rock. The reservoir is highly fractured with 1–2% fracture porosity. The matrix rock has low permeability, and the dominant pore fluid in the bulk of the reservoir is liquid water. For such a material this seemingly low value of K can be reconciled with the much higher dynamic bulk modulus K_d determined from seismic propagation velocities.

Earthquakes at The Geysers appear to be influenced by volume strain. There is a correlation between those parts of The Geysers geothermal field that show large volume strain and the initiation and location of seismic activity. However, there does not seem to be a simple relationship between strain and number of events.

Acknowledgments. The fieldwork involved in this study was not always pleasant, so our thanks go to all those who helped in the field: Carl Chang, Doug Dodge, Patti (Maria-Giovanna) Guatteri, Mark Holloway, Monique Jaasma, Shelley Kenner, Dave Lessick, Ian Manger, Mark Murray, Susan Owen, Mike Poland and Ellen Yu. We are also grateful for the help given by the employees of Calpine, CCPA, NCPA and Unocal, and by Ali Khan of DOGGR. Mike Carpenter and Roger Denlinger kindly provided maps and data from the earlier leveling surveys.

We also thank the two anonymous reviewers and the JGR editor for their time and efforts on our behalf. This research was supported by the DOE Office of Basic Energy Sciences.

References

Arnadottir, T., P. Segall, and M. Matthews, Resolving the discrepancy between geodetic and seismic fault models for the 1989 Loma Prieta, California, earthquake, *Bull. Seismol. Soc. Am., 82*, 2248–2255, 1992.

Barker, B.J., M.S. Gulati, M.A. Bryan, and K.L. Reidel, Geysers reservoir performance, in *Monograph on the Geysers Geothermal Field, Spec. Rep. 17*, pp. 167–178, Geotherm. Resour. Counc., Davis, Calif., 1992.

Denlinger, R.P., W.P. Isherwood, and R.L. Kovach, Geodetic analysis of reservoir depletion at The Geysers steam field in northern California, *J. Geophys. Res., 86*, 6091–6096, 1981.

Eberhart-Phillips, D., and D.H. Oppenheimer, Induced seismicity in The Geysers geothermal area, California, *J. Geophys. Res., 89*, 1191–1207, 1984.

Evans, K.F., T. Kohl, L. Rybach, and R.J. Hopkirk, The effects of fracture normal compliance on the long term circulation behavior of a Hot Dry Rock reservoir: A parameter study using the new fully-coupled code FRACTure, *Trans. Geotherm. Resour. Counc., 16*, 449-556, 1992.

Gunderson, R.P., Porosity of reservoir graywacke at The Geysers, in *Monograph on the Geysers Geothermal Field, Spec. Rep. 17*, pp. 89–93, Geotherm. Resour. Counc., Davis, Calif., 1992.

Hill, D., J.P. Eaton, and L.M. Jones, Seismicity, 1980-86, in *The San Andreas Fault System, California, U.S. Geol. Surv. Prof. Pap., 1515*, 115-151, 1990.

Hofmann-Wellenhof, B., H. Lichtenegger, and J. Collins, *GPS Theory and Practice*, 3rd rev. ed., Springer-Verlag, Wien, 1994.

Kern, H., Elastic wave velocities and constants of elasticity of rocks at elevated pressures and temperatures, in *Physical Properties of Rocks*, vol 1b, edited by G. Angenheister, Springer-Verlag, New York, 1982.

Langbein, J., F. Wyatt, H. Johnson, D. Harmann, and P. Zimmer, Improved stability of a deeply anchored geodetic monument for deformation monitoring, *Geophys. Res Lett., 22*, 3533–3536, 1995.

Leick, A., *GPS Satellite Surveying, 2nd edition* Wiley–Interscience, New York, 1992.

Lofgren, B.E., Monitoring crustal deformation in the geyser-clear lake region. in *Research in The Geysers-Clear Lake Geothermal Area, Northern California, U.S. Geol. surv. Prof. Pap. 1141*, 136–146, 1981.

Matthews, M.V., and P. Segall, Estimation of depth-dependent fault slip from measured surface deformation with application to the 1906 San Francisco earthquake, *J. Geophys. Res., 98*, 12153 12163, 1993.

Mavko, G., T. Mukerji, and J. Dvorkin, *Rock Physics Handbook*, Rock Phys. Lab., Stanford Univ., Stanford, Calif., 1996.

Milbert, D.G., and D.A. Smith, Converting GPS height into NAVD88 elevation with the GEOID96 geoid height model, in *Proceedings of GIS/LIS '96 Annual Conference and Exposition, Denver,* pp. 681–692, Am. Congr. on Surv. and Mapp., Washington, D.C., 1996.

Mossop, A.P., and P. Segall, Subsidence at The Geysers geothermal field, N. California from a comparison of GPS and leveling surveys, *Geophys. Res. Lett., 24*, 1839 1842, 1997.

Nur, A., and J.D. Byerlee, An exact effective stress law for elastic deformation of rock with fluids, *J. Geophys. Res., 76*, 6414–6419, 1971.

O'Connell, D.R.H., and L.R. Johnson, Progressive inversion for hypocenters and P wave and S wave velocity structure: application to The Geysers, California, geothermal field, *J. Geophys. Res., 96*, 6223–6236, 1991.

Okada, Y., Internal deformation due to shear and tensile faults in a half-space, *Bull. Seismol. Soc. Am., 82*, 1018–1040, 1992.

Parker, R.L., *Geophysical Inverse Theory*, Princeton Univ. Press, Princeton, N.J.,1994.

Wahba, G., *Spline Models for Observational Data*, Soc. for Ind. and Appl. Math., Philadelphia, Pa., 1990.

Webb, F.H., and J.F. Zumberge, An Introduction to GIPSY/OASIS II, *Rep. JPL D–11088*, Jet Propul. Lab., Pasadena, Calif., 1995.

Williamson, K.H., Development of a reservoir model for The Geysers geothermal field, in *Monograph on the Geysers Geothermal Field, Spec. Rep. 17*, pp. 179–187, Geotherm. Resour. Counc., Davis, Calif., 1992.

Zhang, J., Y. Bock, H. Johnson, P. Fang, S. Williams, J. Genrich, S. Wdowinsk, and J. Behr, Southern California permanent GPS geodetic array: Error analysis of daily position estimates and site velocities. *J. Geophys. Res., 102*, 18035–18055, 1997.

A. Mossop, Institut de Physique du Globe de Paris, 4 Place Jussieu, 75252 Paris cedex 05, France. (email: mossop@ipgp.jussieu.fr)

P. Segall, Department of Geophysics, Stanford University, Stanford, CA 94305. (email: segall@geo.stanford.edu)

(Received February 10, 1999; revised June 22, 1999; accepted August 12, 1999.)